micro

MDPI

Article

Designing Viscoelastic Gelatin-PEG Macroporous Hybrid Hydrogel with Anisotropic Morphology and Mechanical Properties for Tissue Engineering Application

Kamol Dey [1,2,*], Silvia Agnelli [2] and Luciana Sartore [2]

[1] Bio-Nanomaterials and Tissue Engineering Laboratory (BNTELab), Department of Applied Chemistry and Chemical Engineering, Faculty of Science, University of Chittagong, Chittagong 4331, Bangladesh
[2] Materials Science and Technology Laboratory, Department of Mechanical and Industrial Engineering, University of Brescia, Via Branze 38, 25123 Brescia, Italy; luciana.sartore@unibs.it (L.S.)
* Correspondence: kamoldey@cu.ac.bd or kamolacct@gmail.com

Abstract: The mechanical properties of scaffolds play a vital role in regulating key cellular processes in tissue development and regeneration in the field of tissue engineering. Recently, scaffolding material design strategies leverage viscoelasticity to guide stem cells toward specific tissue regeneration. Herein, we designed and developed a viscoelastic Gel-PEG hybrid hydrogel with anisotropic morphology and mechanical properties using a gelatin and functionalized PEG (as a crosslinker) under a benign condition for tissue engineering application. The chemical crosslinking/grafting reaction was mainly involved between epoxide groups of PEG and available functional groups of gelatin. FTIR spectra revealed the hybrid nature of Gel-PEG hydrogel. The hybrid hydrogel showed good swelling behavior (water content > 600%), high porosity and pore interconnectivity suitable for tissue engineering application. Simple unidirectional freezing followed by a freeze-drying technique allowed the creation of structurally stable 3D anisotropic macroporous architecture that showed tissue-like elasticity and was capable of withstanding high deformation (50% strain) without being damaged. The tensile and compressive modulus of Gel-PEG hybrid hydrogel were found to be 0.863 MPa and 0.330 MPa, respectively, which are within the range of normal human articular cartilage. In-depth mechanical characterizations showed that the Gel-PEG hybrid hydrogel possessed natural-tissue-like mechanics such as non-linear and J-shaped stress-strain curves, stress softening effect, high fatigue resistance and stress relaxation response. A month-long hydrolytic degradation test revealed that the hydrogel gradually degraded in a homogeneous manner over time but maintained its structural stability and anisotropic mechanics. Overall, all these interesting features provide a potential opportunity for Gel-PEG hybrid hydrogel as a scaffold in a wide range of tissue engineering applications.

Keywords: gelatin; PEG; hybrid hydrogel; biomaterial; scaffold; tissue-like mechanics; stress softening; stress relaxation; cyclic compression; tissue engineering

check for updates

Citation: Dey, K.; Agnelli, S.; Sartore, L. Designing Viscoelastic Gelatin-PEG Macroporous Hybrid Hydrogel with Anisotropic Morphology and Mechanical Properties for Tissue Engineering Application. *Micro* **2023**, *3*, 434–457. https://doi.org/10.3390/micro3020029

Academic Editors: Laura Chronopoulou and Yujie Chen

Received: 22 January 2023
Revised: 24 February 2023
Accepted: 28 March 2023
Published: 11 April 2023

Copyright: © 2023 by the authors. Licensee MDPI, Basel, Switzerland. This article is an open access article distributed under the terms and conditions of the Creative Commons Attribution (CC BY) license (https://creativecommons.org/licenses/by/4.0/).

1. Introduction

Everyday, thousands of people of all ages across the world are admitted to hospitals because of the severe injuries or malfunctions of some vital organs [1]. Organ or tissue transplantation is a standard therapy to treat these patients. It is ironic that many of these people will die due to the paucity of donor organs and high processing cost involved in organ transplantation [2]. Realizing the extreme organ transplant shortage worldwide, the WHO (World Health Organization, Geneva, Switzerland) quotes 'If we are prepared to receive a transplant should we need one, then we should be ready to give' on its official website [3]. Yet, the gap between increasing demand and supply of organs is still widening. To meet this global clinical need, tissue engineering that integrates biology with engineering has emerged to regenerate injured or diseased tissues and organs within/outside the body [1].

Biomaterial, a central aspect of tissue engineering, serves as a three-dimensional (3D) scaffold capable of copying the structural, physical, chemical, mechanical and biological features of the natural extracellular matrix (ECM) to support cells as well as guiding them toward a specific tissue construct [1,4]. Recently, hydrogel—a crosslinked 3D polymeric network with an excellent ability to mimic the native ECM functionalities of the human body—has evolved as a potential scaffold for controlling/guiding cell fate toward a specific tissue/organ [5–7]. Besides executing excellent biodegradability and biocompatibility, hydrogels can practically be cast into any shape and size and can be formed typically under cyto-compatible conditions for creating a cell-supportive environment [4]. Despite these outstanding advantages of hydrogels, they have several drawbacks including inferior mechanical properties (low stiffness and strength), difficulty in sterilization and being tough to handle during biological experiments [4,8]. One promising strategy to improve the mechanical properties of hydrogels is crosslinking with suitable crosslinkers with low/nil cytotoxicity. However, the selection of proper crosslinkers as well as hydrogel-forming base polymers is of utmost importance for tissue engineering application [4].

Among numerous scaffolding materials, biopolymer-based hydrogels are considered one of the most suitable candidates for constructing tissue engineering scaffolds owing to their unique physicochemical properties (such as inherent biological activity, natural cellular adhesion sites, excellent biodegradability that is favorable for tissue remodeling, etc.) and excellent biocompatibility [9]. However, as a critical limitation, these biopolymer-derived hydrogels do not always provide favorable physicochemical properties such as mechanical robustness and load-bearing capability, resistance to compressive forces and the suitable degradation timeframe required for optimal cell growth [4,9,10]. In this regard, hybrid hydrogels have received huge scientific attraction in biomedical applications due to their excellent versatile properties such as better capturing the multifunctional nature of native ECM, offering opportunities to tailor specific material properties and improving mechanical robustness of the hydrogel as well as enhancing the delivery of therapeutics [11,12]. Among them, hybrid hydrogels with anisotropic morphology and mechanical properties are of intense interest in tissue engineering because of their mimicking hierarchically anisotropic structures and mechanical properties of natural tissues such as skin, tendon, muscle, articular cartilage, heart, etc. [13–18]. The anisotropy of biological systems often plays a vital role in mass transport, surface lubrication and force generation. It is reported that anisotropic structures of the cultivation media greatly influence cell proliferation, migration and differentiation [18–23]. However, most synthetic hydrogels are isotropic in terms of morphology and mechanical properties, which are substantially different from the biological systems. Conceptually, copying more cues from nature (biological tissue) and incorporating them into a hybrid hydrogel system in a benign and sustainable way would be an appealing approach [11]. Motivated by this, recently, researchers have paid much attention to designing and developing biopolymer-based hydrogels with previously unattainable favorable physico-mechanical properties under a congenial and sustainable approach.

The present study attempts to design a biomimetic hybrid hydrogel, consisting of gelatin (Gel) and polyethylene glycol (PEG) polymers, with anisotropic structural and mechanical properties using functionalized PEG as a crosslinker whose end epoxide groups dominantly react with the free lysine α-amino group of gelatin. Biopolymer gelatin—a denatured protein obtained by hydrolysis of animal collagen with either acid or alkaline—is one of the most remarkable candidates for hydrogels due to its cell-adhesive structure, low cost, availability, high biocompatibility, biodegradability, low immunogenicity and accessible functional groups that allow facile chemical modifications with other biomaterials or biomolecules [4]. On the other hand, PEG—a hydrophilic synthetic polymer with two hydroxyl end groups—is widely used in biomedical application because of its good biocompatibility, non-immunogenicity and resistance to protein adsorption [24]. Although structurally and mechanically anisotropic, hydrogel can be prepared by imparting a specific orientation of nanofillers, pores, fibrous networks and groove/ridge topographies which

leverage magnetic or electric stimulation, electrospinning, 3D printing or unidirectional freeze-casting, [25–34]; however, the clinical translation of these hydrogels is impeded due to their strict, complex and cumbersome preparation processes, high cost, cytotoxicity, difficulty in terminal sterilization and lack of scalability [29]. Moreover, controlling the pore size and wall thickness of the anisotropic hydrogel is also important for tissue engineering application [28]. While 3D printing or electrospinning approaches are potential tools to fabricate the anisotropic ordered structure, they require specialized instruments and personnel as well as taking a prolonged time, making them less attractive from a practical point of view [26,35]. Moreover, these approaches lack the versatility of incorporating a wide range of materials to create complex 3D structures [26]. In addition, an extrinsic field (magnetic or electric) produces an anisotropic aligned structure; however, a requirement in applying a prolonged intense extrinsic magnetic field to impart ordered structure limits its widespread application [26,35]. In addition, electric or magnetic stimulations fail to control the pore size of the hydrogel over a wide range (5 to 400 μm). In contrast, unidirectional freeze-drying is an effective technique that offers good control over the pore size and wall thickness of the anisotropic hydrogel [28]. Noted that, beyond just introducing anisotropic architecture through a freeze-drying approach, the underpinning processing conditions need to be green, mild, versatile and scalable for practical biomedical application. The aim and objective of this present work is to fabricate a structurally stable 3D anisotropic hybrid hydrogel based on gelatin via a green, simple, scalable and cost-effective synthesis procedure for tissue engineering application. Moreover, we attempt to highlight how hydrolytic degradation affects the mechanical anisotropy of the hydrogel. Here, we employed a simple uniaxial freezing process with liquid nitrogen followed by freeze-drying under vacuum (lyophilization) to obtain structurally stable 3D porous anisotropic hydrogels that provide suitable hydrolytic resistance and possess natural tissue-like mechanical properties as well. The in-depth mechanical characterization (both tensile and compressive modes) of the hybrid hydrogel was outlined. To the best of our knowledge, this is the first report of its type showing how hydrolytic degradation affects the mechanical anisotropy of the hydrogel.

2. Materials and Methods

2.1. Materials

Pharmaceutical grade Type A gelatin (produced from pig skin, 280 bloom, viscosity 4.30 mPs) was obtained from ITALGELATINE, Santa Vittoria d'Alba, Italy. Poly(ethylene glycol)diglycidyl ether (PEGDGE) (molecular weight 526 Da) was purchased from Sigma-Aldrich Co (Milan, Italy). Ethylene diamine (EDA) was supplied by Fluka, Milan, Italy. All materials were used without further purification.

2.2. Methods

2.2.1. Formation of Gel-PEG Hybrid Hydrogel

We prepared the anisotropic macroporous hybrid hydrogel using a simple direction-dependent freeze-drying technique. Briefly, gelatin (6 g) was dissolved in 65 mL distilled water at 45 °C under mild magnetic stirring followed by the addition of 1.4 g functionalized PEG (as a crosslinker) and, subsequently, 70 mg EDA. The reaction mixture (pH between 7 and 7.5) was gently stirred at 45 °C for 1 h, poured into the glass plate and then allowed to form a gel for 1 h at room temperature. The obtained gel was carefully peeled off, cut into rectangular bars (5 cm × 1 cm × 1 cm) and placed into a pyrex crystallizing dish. The direction-dependent freezing was performed by resting the crystallizing dish on the surface of an 8 cm-deep pool of liquid nitrogen, enabling freeze-casting at −196 °C (Figure 1a). The gel was incubated for 30 min at the freezing temperature to ensure complete freezing, which was assessed visually. During the evaporation of liquid nitrogen, the gel was unidirectionally frozen from the bottom to the top (Figure 1b). After that, the frozen gel was transferred to the freeze-dryer (lyophilizer) for the sublimation of ice crystals. We maintained a temperature of −60 °C and a pressure of 0.5 mbar throughout

the freeze-drying process, which resulted in an anisotropic porous aerogel. Finally, the porous aerogel was post-cured at 45 °C for 2 h in the oven under vacuum to complete the crosslinking/grafting reaction in the dried condition. The aerogel was washed several times with distilled water at 37 °C to eventually remove the unreacted reagents and dissolved components and again freeze-dried in a lyophilizer.

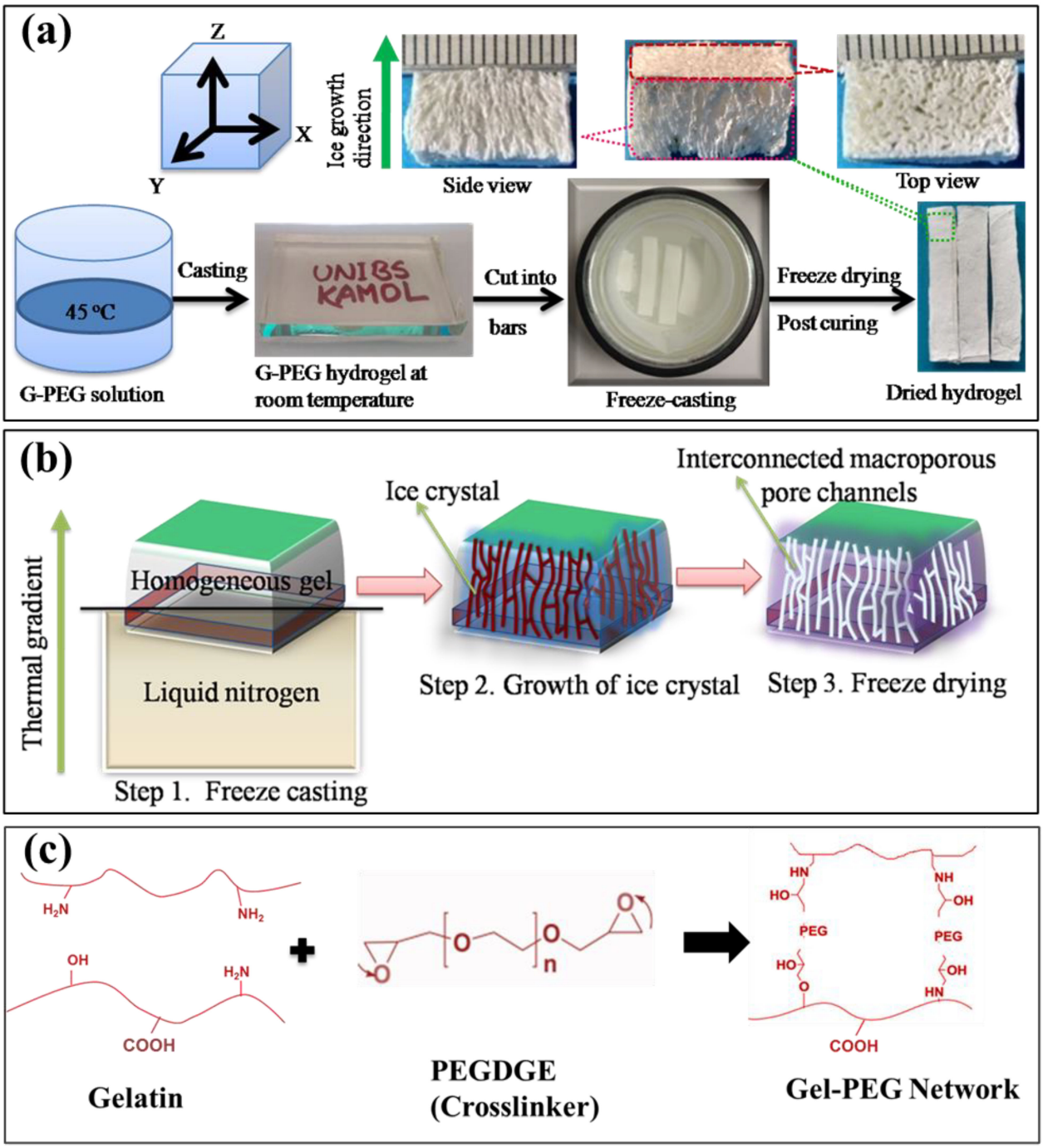

Figure 1. Schematic representation of the synthesis of macroporous Gel-PEG hydrogel: (**a**) simplified form of hydrogel preparation process, (**b**) formation of macroporous interconnected channels along the direction of freezing and (**c**) proposed mechanism showing the Gel-PEG stable network formation.

2.2.2. Physical Properties Measurements

Gel Fraction of Gel-PEG Hybrid Hydrogel

The samples were washed in distilled water several times at 37 °C for 24 h. The gel fraction was calculated following the below equation:

$$\text{Gel fraction } (\%) = \frac{M_d}{M_o} \times 100 \quad (1)$$

where, M_o is the initial dry mass of the sample and M_d is the dry mass of the sample after washing.

Measurement of Apparent Density and Porosity of the Gel-PEG Hybrid Hydrogel

The apparent density and porosity of the dried hybrid hydrogel were measured using the ethanol displacement method with minor modifications as described elsewhere [36]. The entrapped air of the hydrogel was removed under vacuum before commencing the experiment. At first, the total volume (V_2) of ethanol and hydrogel was recorded by immersing a known mass (M) of the dried hydrogel into a graded cylinder containing a known volume (V_1) of ethanol. The volume difference ($V_2 - V_1$) is equivalent to the volume of the hydrogel skeleton. After that, the hydrogel was carefully removed from the ethanol and the residual volume (V_3) of the ethanol was recorded. The volume difference ($V_2 - V_3$) represented the total volume (V) of the hydrogel. The experiment was repeated five times and the standard deviation of the results was calculated.

The apparent density (ρ) of the hydrogel was evaluated using the following equation:

$$\text{Apparent density } (\rho) = \frac{M}{V_2 - V_3} \quad (2)$$

The porosity (ε) of the hydrogel was determined following the below equation:

$$\text{Porosity } (\varepsilon) = \frac{V_1 - V_3}{V_2 - V_3} \quad (3)$$

Swelling Ratio (%) of Gel-PEG Hybrid Hydrogel

The swelling ratio (%) of the hydrogel was evaluated by soaking the pre-massed samples in distilled water at 37 °C over a period of 7 days. The wet sample was taken out from the distilled water at each fixed time interval. The excess surface water was removed by gently pressing with tissue paper and then weighed precisely using an electronic analytical balance. The swelling ratio was expressed as the ratio of weight water uptake by the sample ($M_t - M_o$) to the initial dry weight of the sample (M_o) and the following equation was used:

$$\text{Swelling ratio } (\%) = \frac{M_t - M_o}{M_o} \times 100 \quad (4)$$

where, M_t and M_o are the masses of the wet and dry samples, respectively. The swelling experiment was carried out using five samples, and the standard deviation of the results was calculated.

2.2.3. Structural Characterization

Fourier transform infrared (FTIR) spectroscopy (Thermo Scientific, Madison, WI, USA, Nicolet iS50 FTIR spectrophotometer equipped with a PIKE MIRacle attenuated total reflectance attachment) was used to find the characteristic chemical groups' presence in the starting components and hybrid hydrogel. FTIR spectra were obtained within a range between 4000 and 400 cm^{-1} at a resolution of 4 cm^{-1}.

2.2.4. Morphological Analysis (Stereomicroscope and SEM)

The surface morphology of the hydrogel was analyzed using both an optical microscope and a scanning electron microscope (SEM). For optical microscopic visualization, the dried samples were cut in a parallel direction (direction of ice crystal growth) perpendicular to the macroporous channels, and the morphologies of the surfaces and textures were observed in both directions using a stereomicroscope (LEICA DMS 300, Leica Microsystems GmbH, Wetzlar, Germany) with reflected light. In the case of SEM analysis, the samples were sputter coated with gold nanoparticles using a sputter coater. The morphology was analyzed at an accelerating voltage of 10 kV at various magnifications using an SEM Cambridge scanning electron microscope.

2.2.5. Mechanical Properties of the Gel-PEG Hybrid Hydrogel

A universal testing system (INSTRON series 3366) was used to perform the mechanical tests in both the tensile and compressive moods of the hydrogel. A 50 N load and a crosshead rate of 10 mm/min were used for both modes. For the tensile test, the samples were cut from the hydrogel into dumbbell shapes using a die (according to ISO37 type 2), frozen in liquid nitrogen, lyophilized under vacuum and post-cured at 45 °C for 2 h. The elastic modulus (stiffness) was calculated from the initial linear part (1–5% strain) of the stress-strain curve. At least five samples were tested in wet conditions (immersed in distilled water for 2 days), and data were represented as mean ± standard deviation (SD). For a compressive test, prior to testing, the as-prepared hydrogel samples were soaked in distilled water at 37 °C for 48 h. An optical traveling microscope was used to precisely measure the dimension of the samples. A load of 0.01 N was applied to ensure complete contact between the sample surface and plate before starting the compression test. Rectangular-shaped samples were compressed either parallel or perpendicular to the macroporous channels up to a maximum of 50% strain of their original heights. The cyclic successive loading-unloading test was carried out without a resting time for 10 cycles in each direction. The slope of the compressive stress-strain within the range of 5–10% strain of the first compressive cycle was considered as the initial elastic modulus, and the maximum stress at 50% strain was taken as the compressive strength of the hydrogel.

The obtained hysteresis loop area during the cyclic loading-unloading test indicates the viscous nature of the hydrogel. A higher dissipation energy means a higher viscoelastic nature of the hydrogel. The dissipation energy (kJ/m^3) was calculated from the area bounded by the hysteresis loop. The area enclosed by the loading curve and horizontal axis was considered as the compression energy (kJ/m^3), and the relaxation energy (kJ/m^3) was defined as the area bounded between the unloading curve and the horizontal axis. The ratio of dissipation energy (kJ/m^3) to the compression energy (kJ/m^3) was expressed as percentage dissipation energy (%).

To further characterize the mechanical stability of the hydrogel, consecutive cyclic loading-unloading tests with a gradually increasing maximum compressive strain from 20% to 60% strain of the hydrogel at different maximum (20%, 30%, 40%, 50% and 60%) strains were carried out on the same sample without giving resting time between the consecutive loading cycle. The area encircled by the loading and unloading curves in the stress-strain diagram at each maximum strain was considered the dissipation energy (kJ/m^3) of the hydrogel at each maximum strain.

Moreover, a stress relaxation test was performed to evaluate the viscoelasticity of the hydrogel. Viscoelastic material relaxes stress over time at a fixed strain during a stress relaxation test. For evaluating stress-relaxation behavior, the pre-conditioned samples (having already undergone cyclic compression at 50% strain up to 10 cycles and shown no variation in maximum stress after the 5th cycle) were quickly compressed to 15% strain with a deformation rate of 60 mm/min. Then, the variation of stress was recorded over time (up to 20 min) while keeping the strain constant. The percentage stress relaxation and half stress relaxation time (the time by which peak stress becomes half of its value) were calculated. Additionally, the stress relaxation behavior of the hydrogel was performed

when subjected to compression holding at various strain levels (5%, 15%, 30% and 45%) both in parallel and perpendicular directions.

2.2.6. Hydrolytic Degradation of Gel-PEG Hybrid Hydrogel

The hydrolytic mass loss of the hydrogel was carried out by soaking the pre-massed sample (M_i) in distilled water at 37 °C at 7, 14, 21 and 28 days. The samples were removed from the distilled water at a fixed time interval and rinsed with fresh water to remove the loose/adherent residues of the hydrogel. Then, the samples were air-dried at an ambient condition, vacuum-dried at 45 °C for 4 h and, finally, the dried mass (M_f) was measured. The mass loss (%) was calculated using the following equation:

$$\text{Mass loss } (\%) = \frac{M_i - M_f}{M_i} \times 100 \quad (5)$$

In addition, cyclic compression tests were performed during hydrolytic degradation (at 7, 14, 21 and 28 days) in both directions (parallel and perpendicular) to monitor the mechanical integrity of the hydrogels during hydrolytic degradation.

2.2.7. Statistical Analysis

The statistical analysis was carried out by Origin 8.5 Pro. All the data reported were mean ± standard deviation (SD).

3. Results and Discussion

3.1. Formation of Anisotropic Gel-PEG Hybrid Hydrogel

The crosslinking reaction between the gelatin polymer chain and functionalized PEG was carried out using an easy and simple synthetic procedure in an aqueous environment (pH between 7 and 7.5) without using any additives or solvents, as shown in Figure 1a. The procedure used for the preparation of the Gel-PEG hybrid hydrogel is tabulated in Table 1. Crosslinking is a widely used technique to impart structural stability and enhance the mechanical integrity of the gelatin-based hydrogel [4]. We used functionalized PEG (Gel to PEGDGE ratio: 4:1) in gelatin solution to create crosslinking/grafting between end epoxide groups of functionalized PEG and available functional groups (=NH, -NH_2, -COOH and -OH) of gelatin. Epoxy groups of functionalized PEG dominantly reacted with the free lysine α-amino group of gelatin and formed a stable carbon-nitrogen network, as shown in Figure 1c. Gel-PEG hydrogel was found to be transparent upon visual inspection. We adopted a very simple uniaxial freezing technique to impart anisotropic morphology, and the process of forming anisotropic hydrogel is shown in Figure 1a. During the directional freezing of the hydrogel using liquid nitrogen at −196 °C, water molecules crystallized to form an aligned ice crystals template along the freezing direction, and the polymer chains rested in the gaps between them. The freeze-drying process sublimated the ice crystals, leaving behind the interconnected macroporous channels (Figure 1b). The developed synthesis protocol mainly consisted of three steps: (i) crosslinking/grafting between functionalized PEG (PEGDGE) and gelatin chains in an aqueous media which was required to obtain a stable gel before freeze-casting, (ii) a simple unidirectional freezing technique was applied to impart an anisotropic porous network and (iii) a post-curing process (at 45 °C for 2 h) under vacuum was needed to enforce as well as to complete the crosslinking/grafting reaction between the leftover functionalized PEG and gelatin chains. The available hydrophilic groups (=NH, -NH_2, -COOH and -OH) in gelatin segments can bind with water via physical interaction, which limits the occurrence of crosslinking/grafting between PEGDGE and hydrophilic groups. Thus, freeze-drying followed by a post-curing process further facilitated crosslinking/grafting reaction in the solid phase by bringing available functional groups closer. An excess of functionalized PEG over gelatin was employed to obtain adducts with several reactive end groups able to produce crosslinking/grafting with functional groups of gelatin. Moreover, in order to obtain stable hydrogel with good mechanical properties, improved water resistance and an controlled degradation rate,

ethylene diamine (70 mg)—able to react with unreacted epoxy groups—was added. We adopted a two-stage (liquid phase and solid phase (post-curing)) crosslinking/grafting strategy to obtain the maximum degree of crosslinking/grafting. Indeed, the beneficial effect of the curing treatment is often adopted to increase the crosslinking density and reactivity of epoxy functional groups such as those of PEGDGE. As all the reactants were highly water soluble, one might expect that the residual unreacted products could be easily washed off/removed from the dried hydrogel obtained after lyophilization. The use of PEG—an established biomaterial—as a crosslinking agent might provide a certain distance between the linked functional group and the gelatin polymer chains and decrease steric hindrance, which eventually facilitates cell adhesion and triggers cellular responses.

Table 1. Composition and physical properties of the Gel-PEG hydrogel.

	Composition (wt%)		**Physical Properties**		
Sample	**Gelatin (Gel)**	**PEG**	**Apparent Density (g/cc)**	**Porosity (%)**	**Gel Fraction (%)**
Gel-PEG	81	19	0.162 ± 0.01	75.12 ± 2.12	90.30 ± 2.0

FTIR analysis was performed using pure starting materials and hydrogel (washed several times with distilled water at 37 °C and freeze-dried) to characterize the chemical compositions of hydrogel, as shown in Figure 2. The FTIR spectrum of pure functionalized PEG depicted a broad peak at 2875 cm^{-1} related to a C-H stretching vibration. The characteristic intense peak observed at 1096 cm^{-1} is due to C-O stretching (ether bond C-O-C). The pure gelatin showed absorption bands at 3300 cm^{-1} and 2930 cm^{-1}, assigned to amide A and B, respectively, mainly associated with the stretching vibration of –NH groups. The characteristic peaks observed at 1632 cm^{-1}, 1545 cm^{-1} and 1242 cm^{-1} correspond to amide I (due to C=O stretching vibrations), amide II (due to –NH bending vibrations and C-N stretching vibrations) and amide III (due to vibrations in plane of C-N and N-H groups bound amide or vibrations of CH_2 groups of glycine), respectively [8,37]. The peaks at 1081 cm^{-1} and 1033 cm^{-1} indicated a C-O stretching vibration. As shown in the spectra of Gel-PEG hydrogel (shown in the vertical dotted line in Figure 2), all characteristic peaks of individual components were observed in the hydrogel, indicating the formation of a hybrid hydrogel. The intense peak at 1065 cm^{-1} of the hydrogel was due to the incorporation and interaction of functionalized PEG with gelatin and revealed the presence of PEG in the final product.

3.2. Macro and Micro-Structures of Anisotropic Gel-PEG Hybrid Hydrogel

3.2.1. Skin Formation during Freeze-Drying

The freeze-drying technique resulted in the formation of hydrogel with a microporous thin compact skin observed by optical and scanning electron microscopy, as shown in Figure 3. Skin formation is a problem for cell infiltration during culture. However, beneath the thin skin, the sample was highly porous and anisotropic. It is mentionable here that this thin skin, composed of closed compact micropores, could be easily removed by a razor blade to disclose an open porous structure, as noticed from both optical (Figure 3b) and staining microscopy (Figure 3d). This approach allowed us to avoid the problem of skin for cell culture. However, this skin formation might be suitable for another aspect of biomedical application where a one-side-open box-like structure is imperative.

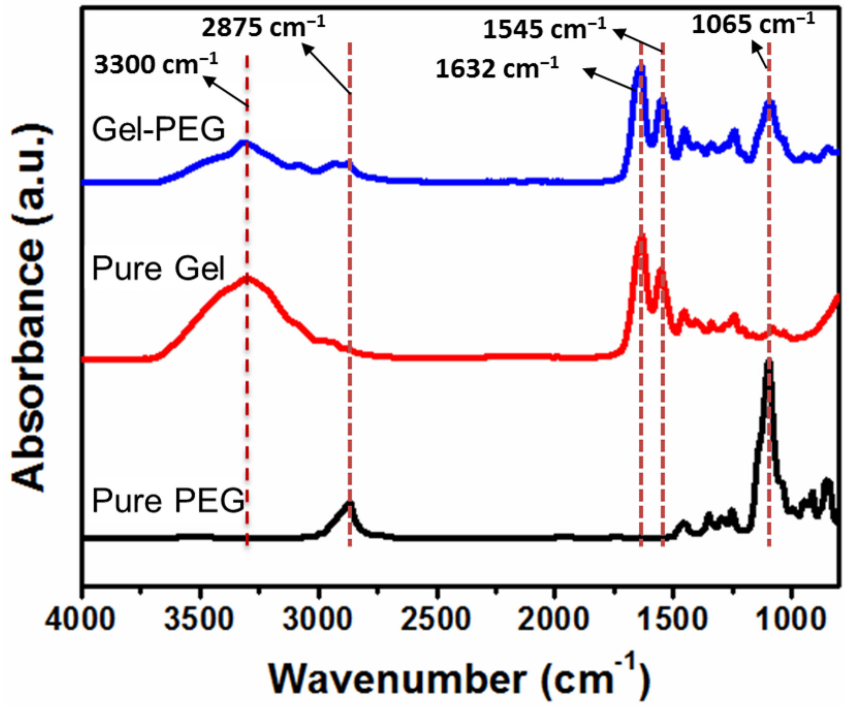

Figure 2. FTIR spectra of pure starting components (Gel, PEG) and Gel-PEG hybrid hydrogel.

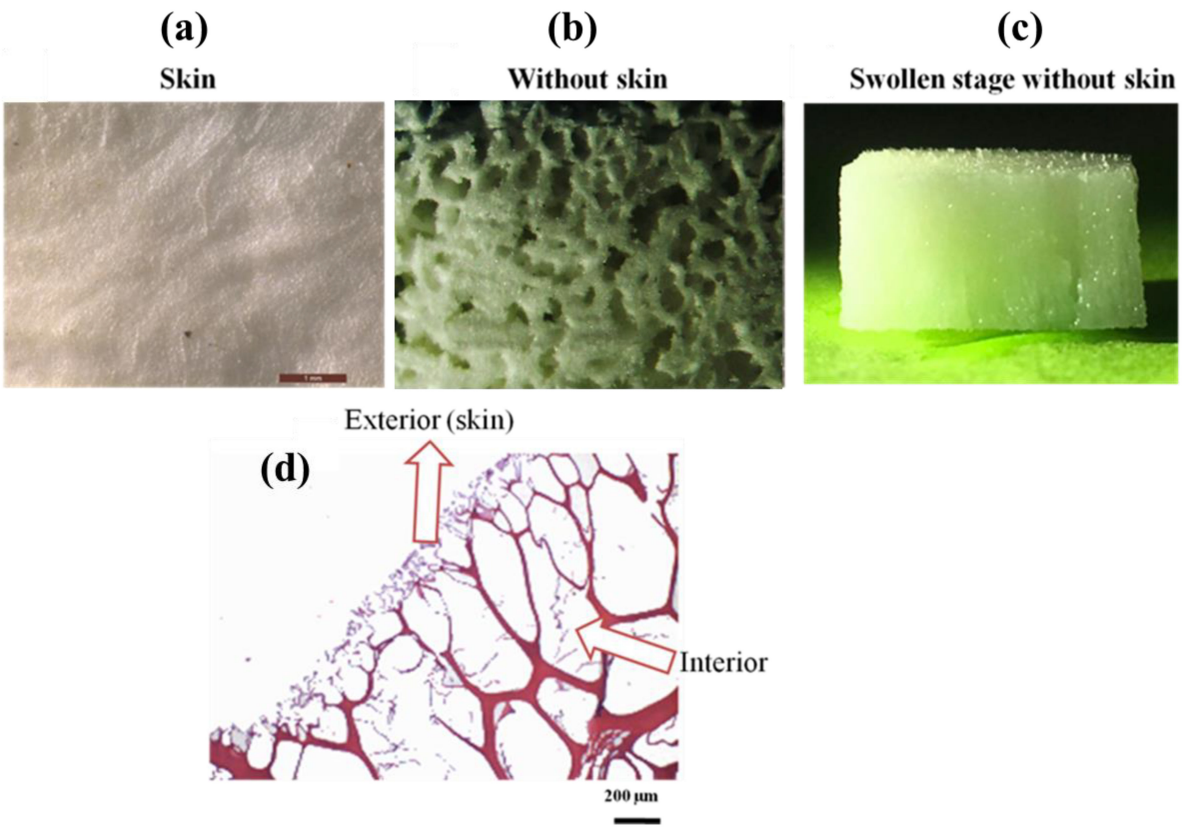

Figure 3. Skin formation during freeze-drying: (**a**,**b**) optical microscopy visualization of hydrogel in dried condition with and without skin, (**c**) hydrogel in swollen stage without skin and (**d**) staining microscopic image of the hydrogel in wet condition showing the thin skin comprising closed pores as well as an interior interconnected open porous structure.

3.2.2. Microscopic Analysis of Gel-PEG Hybrid Hydrogel without Skin

The macro and microstructures of the Gel-PEG hydrogel without skin were investigated using optical and scanning electron microscopes, as shown in Figure 4a–c. It was obvious that the hydrogel showed anisotropic pore structures. The irregular spherical pore morphology was observed in the perpendicular direction of freezing (cross-section) with pore sizes ranging from 20–450 µm (Figure 4b). The macroporous large channels were visible in the parallel direction of freezing (side view). These void channels were connected by large-area lamellae, which were composed of micropores. These micropores on the lamellae and macropores collectively constituted the hierarchical porous architecture. Interestingly, the large lamellae were not isolated but they were interconnected with thin lamella bridges. The distance between lamellae was several tens to more than 200 µm.

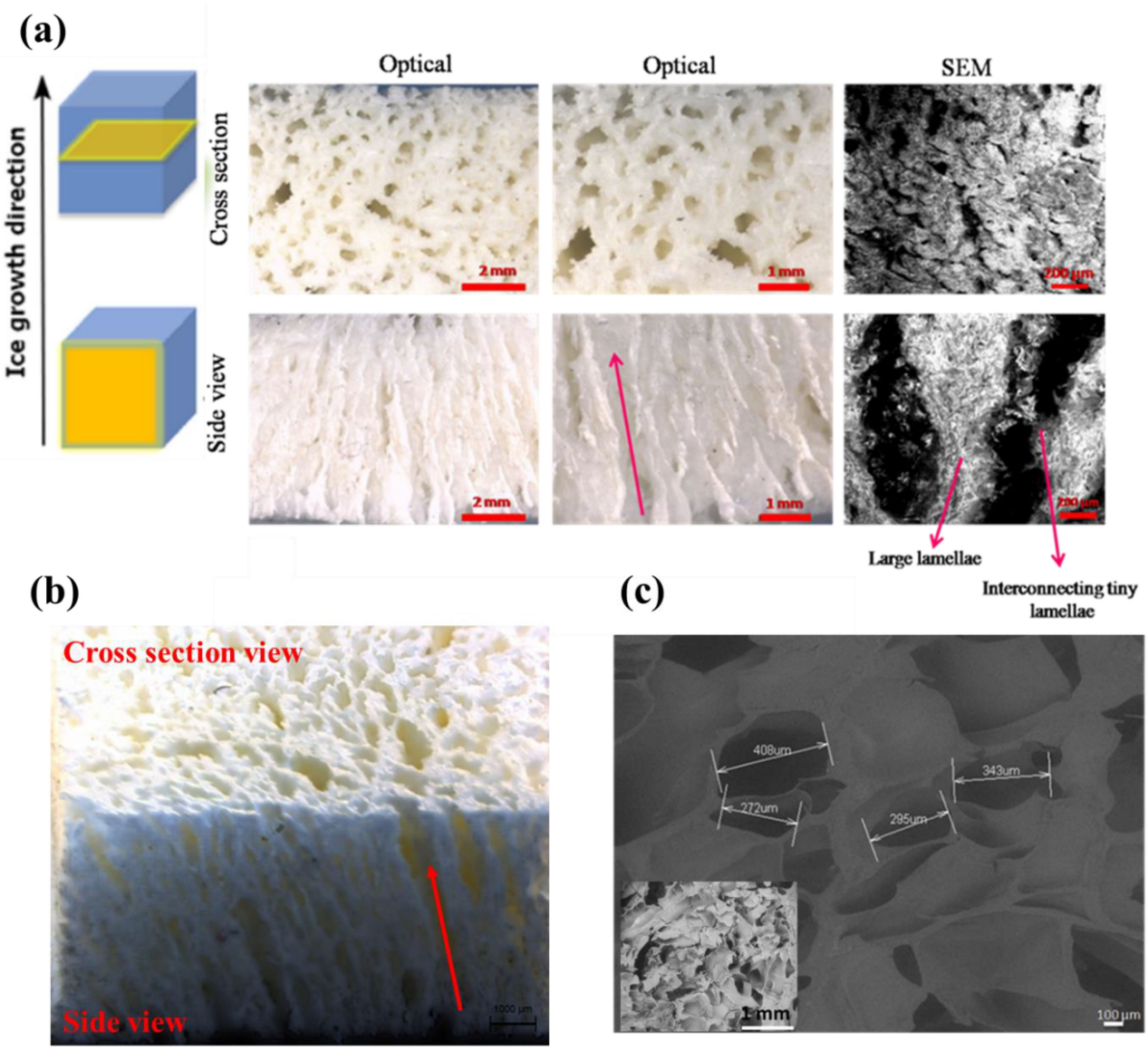

Figure 4. Pore morphology of hydrogel without skin: (**a**) optical and SEM images of the hydrogel. Top and bottom rows show the images of porous structure perpendicular (cross-section) and parallel (side view, the arrow indicates the direction of macroporous channel), respectively, to the direction of ice crystal growth, as depicted in the corresponding cartoons in the left side, (**b**) optical image captured at 45° angle showing anisotropic morphology of the hydrogel and (**c**) SEM image showing distribution of pore sizes of the cross-section area of the hydrogel.

These two distinct pore morphologies, namely, spherical (perpendicular, cross-section view) and lamella (parallel, side view) morphologies are attributed to the anisotropic mass transport phenomenon of the Gel-PEG hybrid hydrogel. Figure 5 depicts the anisotropic dye diffusion through the hydrogel on a macroscopic scale. The diffusion of dye was visualized by monitoring the distance it traveled through the hydrogel. When an aqueous solution of methylene blue was dropped on the hydrogel surface, it diffused preferentially through the large channels (side view).

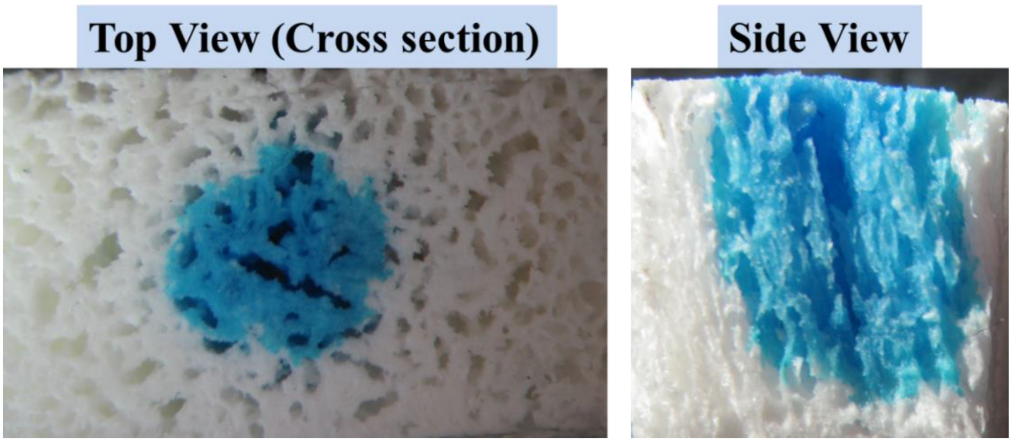

Figure 5. Optical microscopy visualization of anisotropic diffusion of dye through the hydrogel.

3.3. Physical Properties and Swelling Ratio (%) of Gel-PEG Hybrid Hydrogel

Table 1 shows the composition, apparent density and porosity of the Gel-PEG hydrogel. The apparent density of the hydrogel was found to be 0.162 ± 0.01 g/cc, and the hydrogel showed a high porosity of 75.12 ± 2.12%. The gel fraction—defined as the total crosslinked gel eventually washing out un-reacted and soluble components—was found to be 90.30 ± 2.0%.

The swelling ratio is one of the important parameters of hydrogel that is closely correlated to its intrinsic and extrinsic structure, and which instantly gives a preliminary idea of other subsequent characteristics for practical applications. The swelling experiment was conducted by incubating the hydrogel in distilled water at 37 °C for up to 7 days, as shown in Figure 6a. Initially, the hydrogel rapidly absorbed water and reached an equilibrium swelling ratio of 600 ± 8% after 2 days. This high swelling ratio could be beneficial for tissue engineering application.

3.4. Mechanical Properties of Gel-PEG Hybrid Hydrogel

3.4.1. Tensile Mechanical Properties

Mechanical properties of the hydrogel are one of the critical parameters in designing scaffolds for tissue engineering application. Many mechanical cues including bulk stiffness, gradient stiffness, viscoelasticity, mechanical anisotropy, nonlinear elasticity, mechanical confinement and mechanical memory and dosing influence numerous cellular behaviors [5,38]. Consequently, the mechanical properties of the hydrogel were investigated in detail both in tensile and compressive modes. The tensile stress-strain measurements were measured by uniaxial tensile tests using dumbbell-shaped specimens. For the tensile test, the samples were cut from the hydrogel into dumbbell shapes using a die, frozen in liquid nitrogen, lyophilized under vacuum and post-cured at 45 °C for 2 h, as shown in Figure 6b. Figure 6c shows the representative tensile stress-strain curves of the hydrogel in the hydrated condition. The curve was non-linear and J-shaped, similar to those found for native extracellular matrixes. The results as elastic modulus, tensile strength and elongation at break are listed in Table 2.

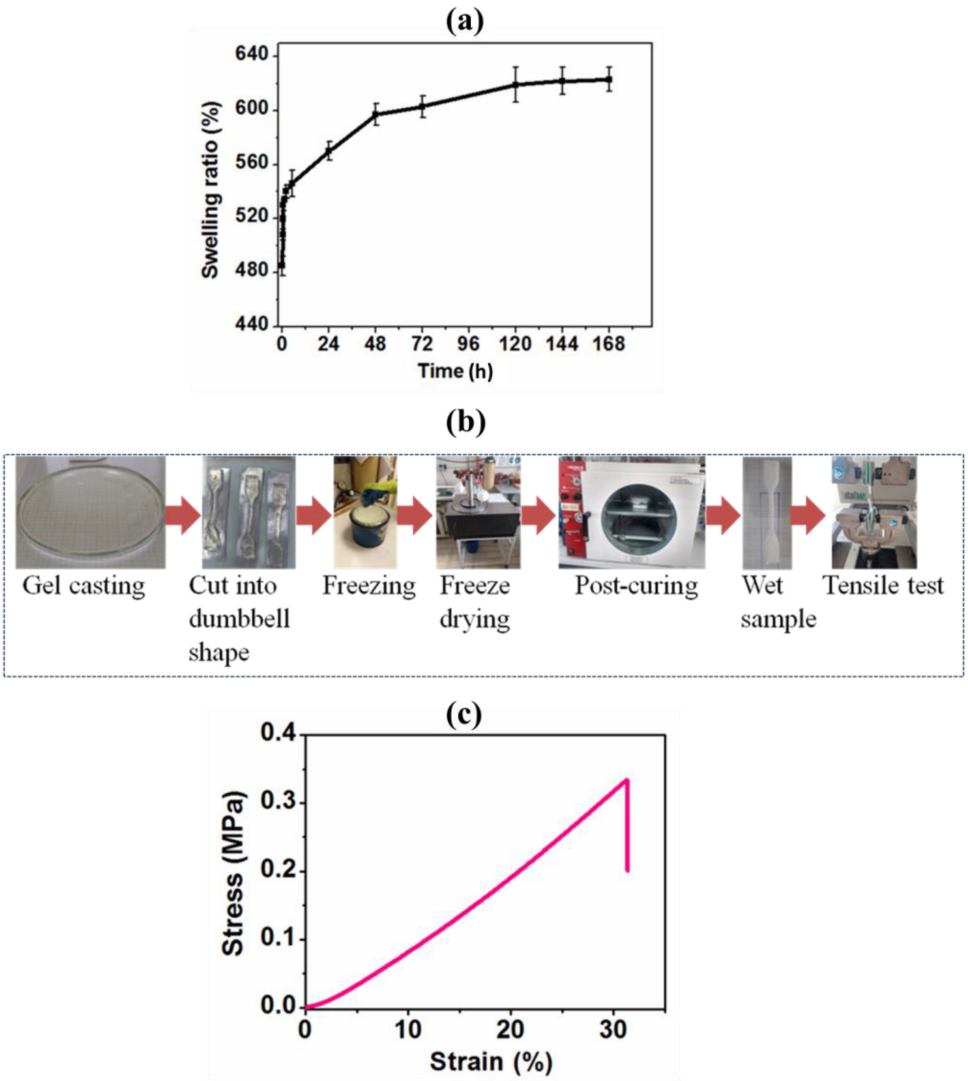

Figure 6. Water uptake and tensile property of the hydrogel: (**a**) swelling ratio of hydrogel incubated in distilled water at 37 °C, (**b**) sample preparation steps for tensile test and (**c**) representative tensile stress-strain curve of the hydrogel.

Table 2. Tensile mechanical properties of the macroporous Gel-PEG hybrid hydrogel.

Tensile Properties	
Tensile elastic modulus (MPa)	0.863 ± 0.13
Tensile strength (MPa)	0.380 ± 0.11
Elongation at break (%)	27.00 ± 4.98

3.4.2. Cyclic Compression and Compressive Mechanical Properties

Consecutive cyclic compression loading-unloading experiments on the wet samples were carried out both parallel and perpendicular to the macroporous channels up to 50% strain for ten cycles without a waiting time. The initial elastic modulus (stiffness) and stress at 50% strain (strength) were calculated from the first loading curve and the energies were measured from the fifth cycle. These values are reported in Table 3. Representative stress-strain curves of the hydrogel compressed parallel and perpendicular to the macroporous channels are shown in Figure 7a. As shown in Table 3 and Figure 7a, the stiffness of the hydrogel compressed in a parallel direction (0.33 ± 0.04 MPa) was significantly higher than that of a perpendicular direction (0.12 ± 0.03 MPa) with an anisotropic ratio of 2.75. The two best plausible ways to explain the increased stiffness when compressed in a

parallel direction might be due to (i) the large lamellae, which act as pillars reinforcing the gels, and (ii) the presence of more entrapped pressurized water between two compressive plates, as in this case, water could not be easily squeezed out in contrast to perpendicular compression. The direction-dependent stiffness of anisotropic hydrogel was correlated with their anisotropic pore structures. However, no significant difference was observed in terms of strength (maximum stress), compression energy (energy applied during loading), relaxation energy (energy recovered during unloading), dissipation energy (area enclosed by loading-unloading curves) and percentage dissipated energy (% ratio of dissipation to compression energy), as revealed in Table 3.

Figure 7b depicts the overall shape of a compressive stress-strain curve compressed in a parallel direction. The stress-strain curve compressed parallel to the macroporous channels clearly showed three distinct regions, namely, an elastic region due to the bending of pore walls and lamellae, a collapsed plateau region as a result of pore walls and lamellae buckling and yielding and a densification region due to the pore walls/lamellae crushing together [39]. On the contrary, the stress-strain curve obtained by perpendicular compression to the macroporous channels showed a non-linear J-shaped curve (Figure 7c). The typical 'shoulder' disappeared because no lamellae buckling phenomenon occurred. When a strain surpassed 40%, the hydrogel observed a strong strain hardening effect, which might be due to the greater densification of the hydrogel because of compressed channels.

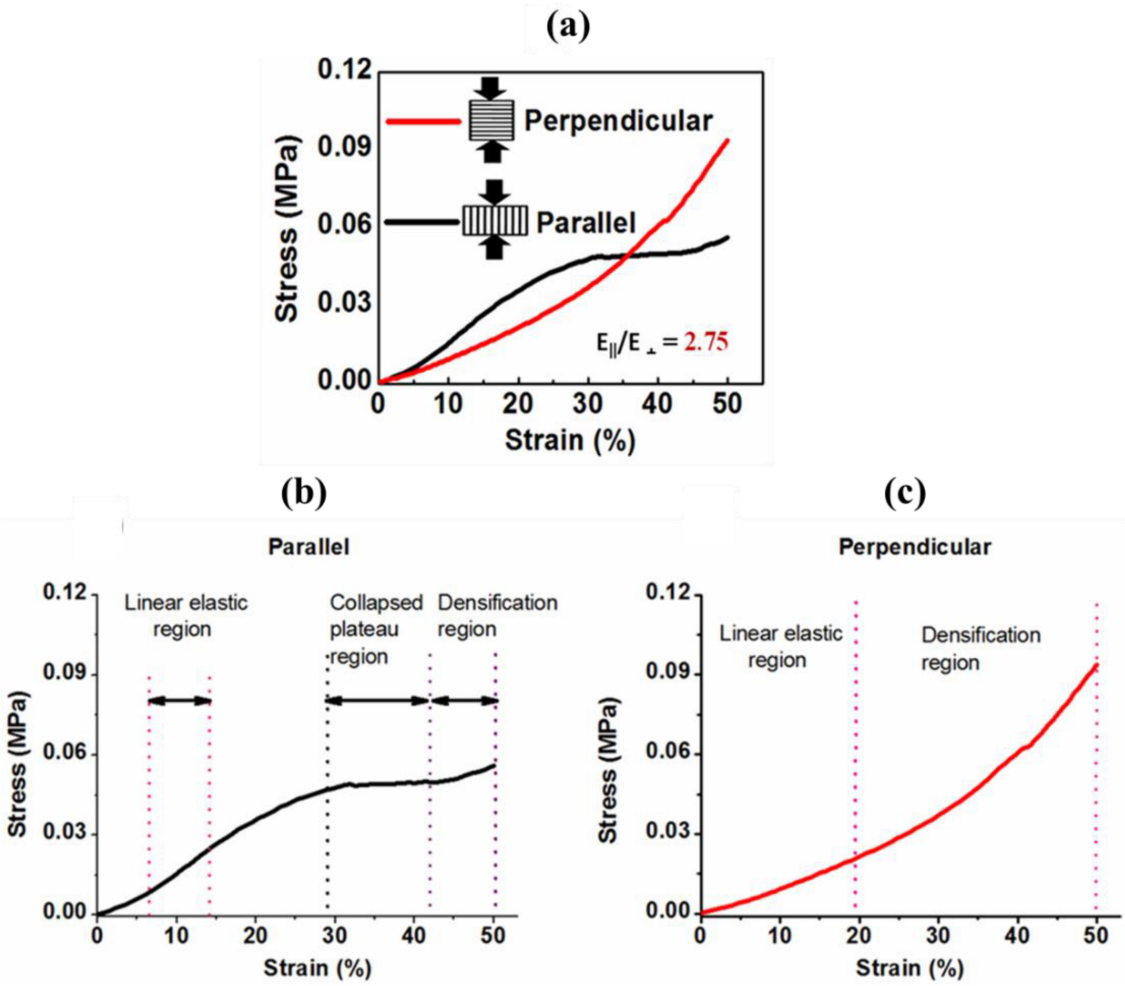

Figure 7. Anisotropic mechanical property of the Gel-PEG hybrid hydrogel: (**a**) representative stress-strain curves of the hydrogel compressed parallel and perpendicular to the macroporous channels, (**b**) the scheme showing three stages of plastic deformation when compressed in a parallel direction and (**c**) the two stages of plastic deformations when compressed in a perpendicular direction.

Table 3. Compressive mechanical properties of the Gel-PEG anisotropic hydrogel in a wet condition (2 days). The compression was performed both parallel and perpendicular to the direction of macroporous channels. The energies were calculated from the fifth cycle. Values were presented as mean ± SD.

Properties	Parallel	Perpendicular
Compressive elastic modulus (MPa)	0.33 ± 0.04	0.12 ± 0.03
Compressive stress (MPa) at 50% strain	0.08 ± 0.02	0.09 ± 0.01
Compression energy (kJ/m^3)	13.73 ± 4.2	14.49 ± 0.5
Relaxation energy (kJ/m^3)	8.71 ± 3.6	9.89 ± 1.2
Dissipation energy (kJ/m^3)	5.03 ± 0.63	4.60 ± 1.2
Percentage of energy dissipation (%)	38.21 ± 7.0	31.76 ± 8.0

Figure 8 represents the consecutive cyclic loading-unloading curves for up to ten cycles at a maximum 50% strain in both directions (parallel: Figure 8a and perpendicular: Figure 8c) and the corresponding stress-time curves without giving any relaxation time during consecutive cycles (parallel: Figure 8b and perpendicular: Figure 8d). The hysteresis loops were observed for all consecutive cycles. All unloading curves returned to a 0% strain, indicating full shape recovery of the hydrogels at 50% deformation. When compressed in a parallel direction, a moderate deviation was shown between the first and second cycles, which indicated that some sort of irreversible damage occurred during the first cycle. We hypothesized that those tiny lamellae bridges connecting large lamellae might be fractured during the first cycle (see side view of SEM images in Figure 4a). However, a slight deviation was noticed during the consecutive second to fifth loading-unloading cycles. After the fifth cycle, all successive hysteresis loops nearly overlapped with each other, indicating that a mechanically stable structure was achieved. Figure 8b shows the corresponding stress-time plot. Clearly, it was observed that the induced stress showed a transient phenomenon: during the first cycle, the induced stress was 0.56 MPa, but during subsequent cycles, it was gradually decreasing and became stationary, reaching a constant value of 0.46 MPa after multiple cycles. This behavior is demonstrated as stress softening (Mullins' effect), which is characterized by lower resulting stress for the same applied strain, often observed in soft-tissue materials where such behavior is known as 'preconditioning' [40]. This 'preconditioning' phenomenon might arise from the collective effects of microfractures, polymeric chain disentanglements, relocation, reordering, and so on, during initial compression loading [40]. In this case also, no variation of compressive stress was observed over time between the fifth cycle and beyond. This indicated that the hydrogel responses during cyclic compression coincided after the fifth cycle, revealing reversible behavior. The surprising result was that tiny lamellae fractures did not allow macroscopic fracture propagation through the hydrogel leading to breakdown, rather than completely returning to the original shape (Figure 8e).

Figure 8c,d shows the stress-time curves resulting from the cyclic loading-unloading and corresponding stress-time curves compressed in a perpendicular direction to the macroporous channels. Stress-strain curves depicted very little variation between the first and second loading curves. However, beyond the second cycle, all subsequent hysteresis loops were superposed, suggesting good reversible behavior. The corresponding stress-time plot also echoed the same scenario (Figure 8d).

We further calculated the dissipation energy of each compression cycle both in parallel and perpendicular directions, and the data are represented in Figure 9a. The hysteresis loop area represented the dissipation energy per unit volume upon deformation. In the case of parallel compression, the hydrogel dissipated huge energy during the first cycle but sharply decreased during the second cycle, which indicated the first loading caused some damage to the hydrogel structure. However, there was no significant difference among the dissipation energies of the fifth and all subsequent cycles. On the contrary, in the case of perpendicular compression, a slightly decreased dissipation energy was observed for the second cycle compared to that of the first cycle; however, beyond the second cycle, the

dissipation energy remained constant. Additionally, as shown in Figure 9b, the percentage of dissipation energies was found to be similar after the fifth to subsequent tenth cycles, further confirming the achieved mechanical stability after a few cycles.

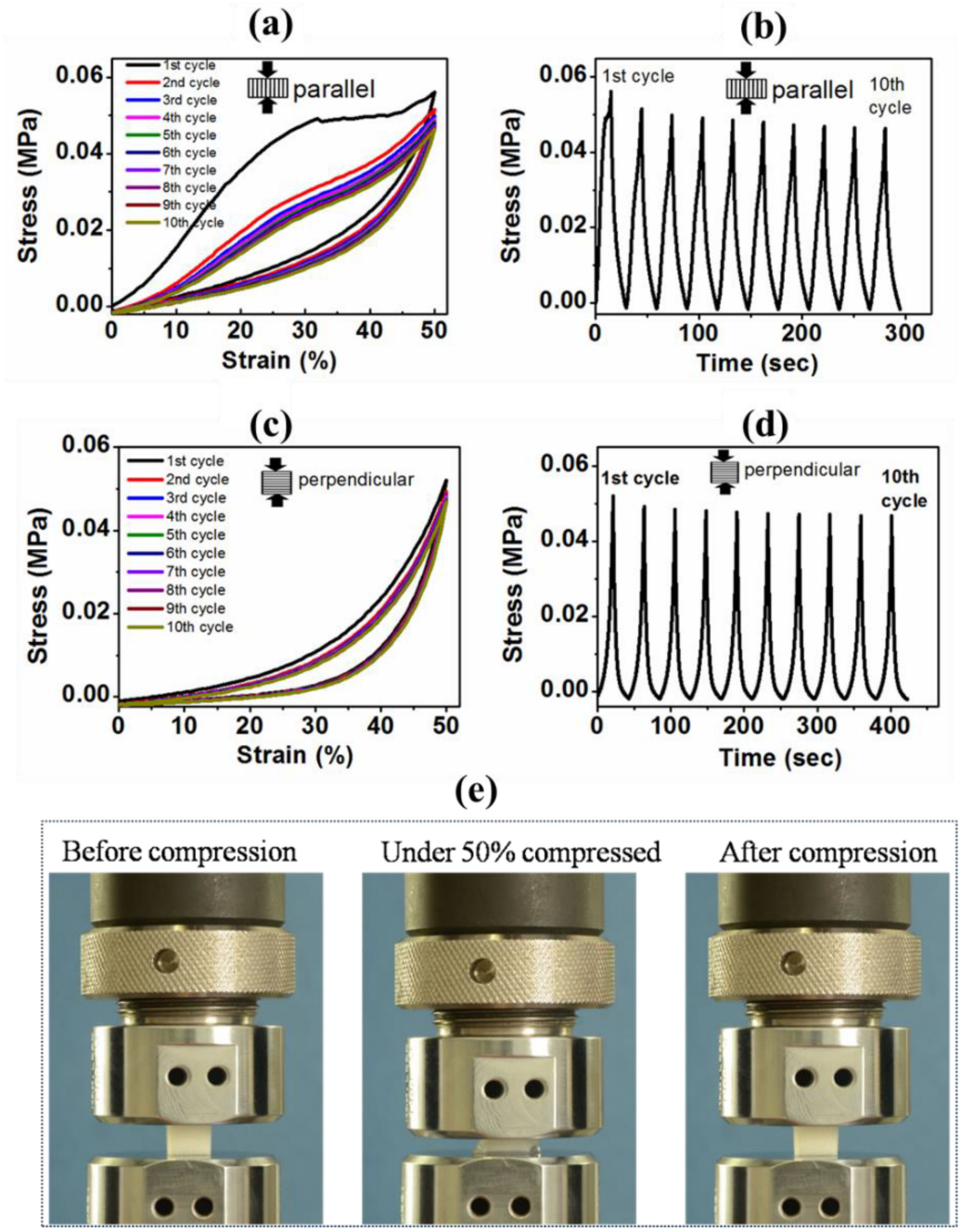

Figure 8. Cyclic compressive mechanical properties of the Gel-PEG hybrid hydrogel: (**a**) cyclic compressive stress-strain curves for up to 10 consecutive cycles at 50% maximum strain without waiting time in parallel and (**c**) perpendicular direction to the macroporous structures of the hydrogels in wet condition, (**b**) the stress-time curves for the corresponding 10 cycles in a parallel direction and (**d**) perpendicular direction, and finally, (**e**) shows the hydrogel undergoing 50% compression and subsequent full shape recovery when the load released to the initial value.

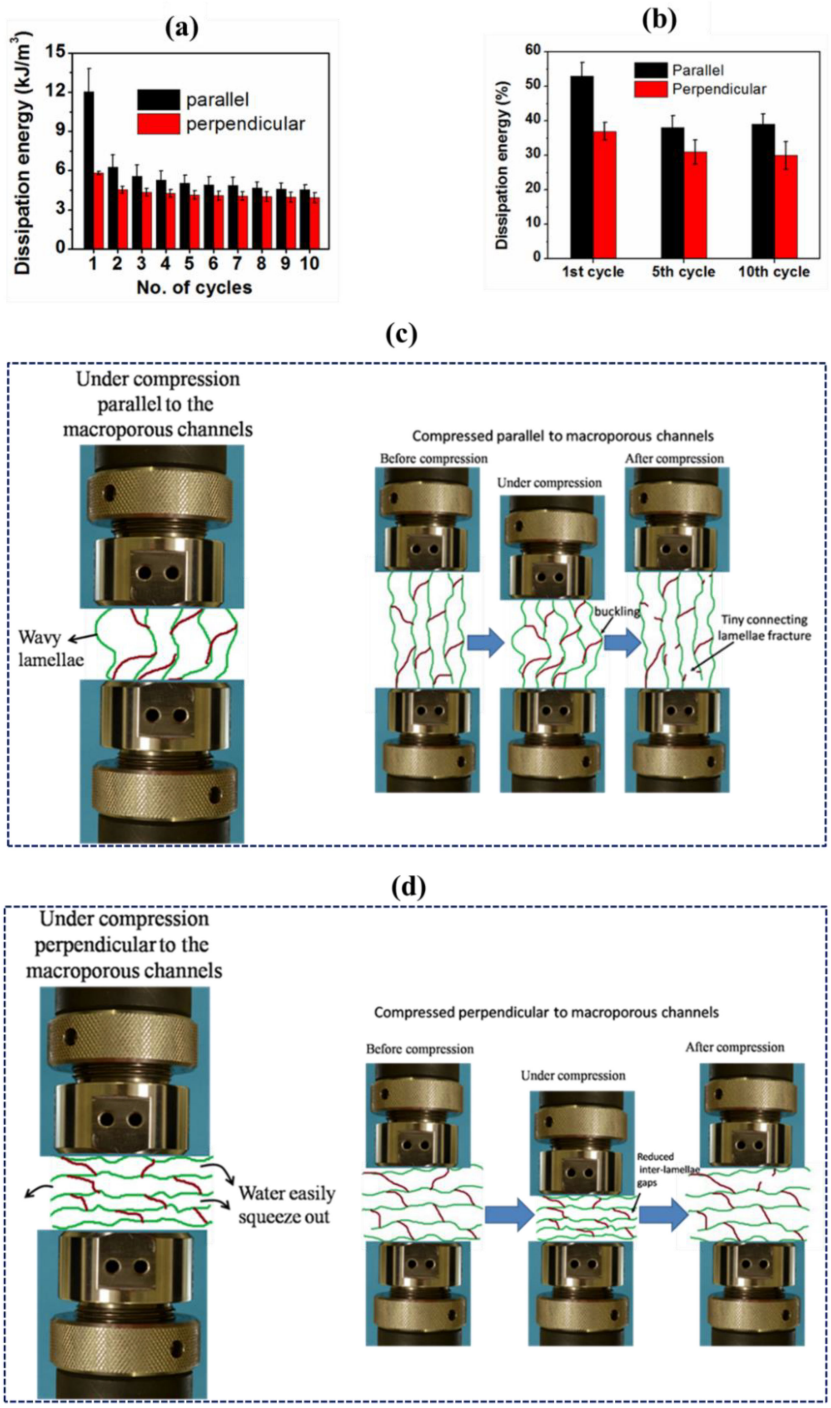

Figure 9. Dissipation energy of the Gel-PEG hydrogel during cyclic compression up to 10 cycles: (**a**) the dissipation energy of each cycle calculated from the area encompassed by loading-unloading curves during successive compression, (**b**) percentage dissipation energies of the 1st, 5th and 10th cycles of the hydrogel subjected to compression both in parallel and perpendicular directions to macroporous channels at 50% maximum strain and (**c**,**d**) schematic illustrations of the sample undergoing compression in parallel and perpendicular to the macroporous channels, respectively.

It is noted that when compressed parallel to the macroporous channels, the calculated dissipation energy and percentage dissipation energy were slightly higher compared to those of a perpendicular direction. The schematic illustrations of the sample undergoing compression parallel and perpendicular to the macroporous channels are displayed in Figure 9c,d. During compression in a parallel direction, interconnected large lamellae

became more wavy, less oriented and caused some microfractures (Figure 9c). Moreover, entrapped water might not easily squeeze out of the sample, resulting in more frictional energy being generated (also dissipated energy due to polymer viscoelasticity). However, during unloading, the lamellae recovered their alignment and orientation. This frictional energy might originate from two distinct paths, forming a hysteresis loop. We postulated that this pronounced buckling and bending of lamellae and more frictional energy due to the migration of more entrapped water might contribute to a larger hysteresis loop area when compressed in a parallel direction. In contrast, during compression in a perpendicular direction, water might easily squeeze out through the macroporous channels, making more available space for the densification of the adjacent lamellae, resulting in fewer microfractures (Figure 9d). These reduced microfractures, polymer deformation and easier water migration within the network might lead to a smaller hysteresis loop area, and, consequently, a lower dissipation energy [4].

To further confirm the mechanical stability of the hydrogel, we also conducted cyclic loading-unloading experiments directly after each other at different maximum strains (20%, 30%, 40%, 50% and 60%) in both directions, and the hysteresis loops were shown in Figure 10a,b. For both cases, the hysteresis loops area became larger with increasing maximum strain. Moreover, as presented in Figure 10c, the hydrogel showed an exponentially increasing trend of dissipation energies with the increasing maximum strain, suggesting that the hydrogel could be capable of effectively dissipating energy at larger deformation. It is noted here that the slightly higher dissipated energies for parallel compression might be due to the migration of more pressurized water throughout the porous network.

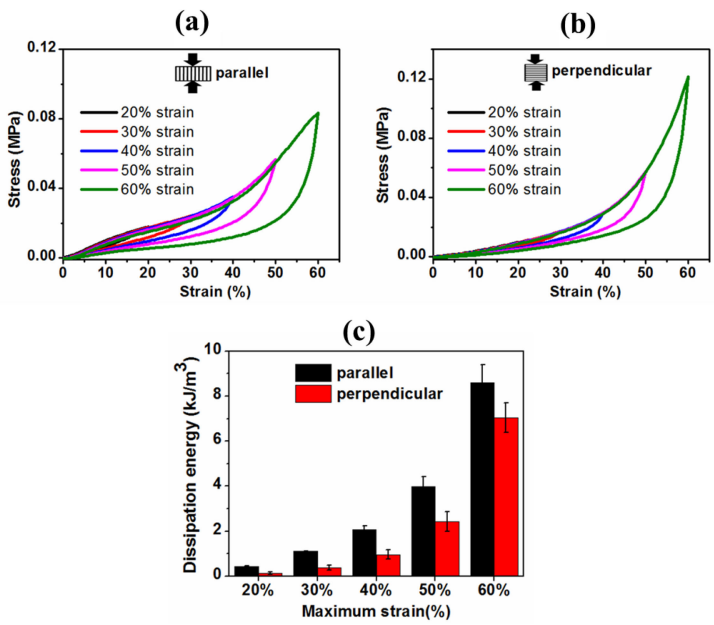

Figure 10. Compressive mechanical properties of the Gel-PEG hybrid hydrogel at different maximum strains: (**a**) the hysteresis loops when compressed in parallel and (**b**) perpendicular to the macroporous channels at different maximum strains and (**c**) corresponding hysteresis energies of the hydrogel compressed in parallel and perpendicular directions.

Collectively, an initially slight reduction in stress and then stabilizing after a few cycles (stress softening effect) and no residuary strain during the consecutive loading-unloading cycles demonstrated elasticity, excellent shape-recovery property, and good mechanical stability of the Gel-PEG hybrid hydrogel.

3.4.3. Stress Relaxation Behavior of the Anisotropic Gel-PEG Hybrid Hydrogel

It is reported that stress relaxation, the ability of the scaffold to dissipate cell-induced forces, is a key mechanical motivator influencing stem cell fate and function [38,41–44]. The

natural extra-cellular matrix is viscoelastic in nature and shows partial stress relaxation [38]. Both degradation and faster stress relaxation represent two synergistic efforts to regulate and improve scaffold performance toward cell culture [41]. Typically, cells exert up to 20–30% strain in 3D cell culture [41]. To assess the viscoelasticity of the Gel-PEG hybrid hydrogel, we performed a stress relaxation test using rectangular-shaped wet samples in both directions. For the stress relaxation test, we applied a constant strain of 15%, as this is the average strain level exerted by cells in 3D cell culture. Prior to commencing the stress relaxation test, the samples were conditioned, then compressed to 15% strain at a strain rate of 60 mm/min and held constant while recording the load as a function of time (20 min), as shown in Figure 11a,b. The samples were quickly compressed to avoid the accumulation of inertia.

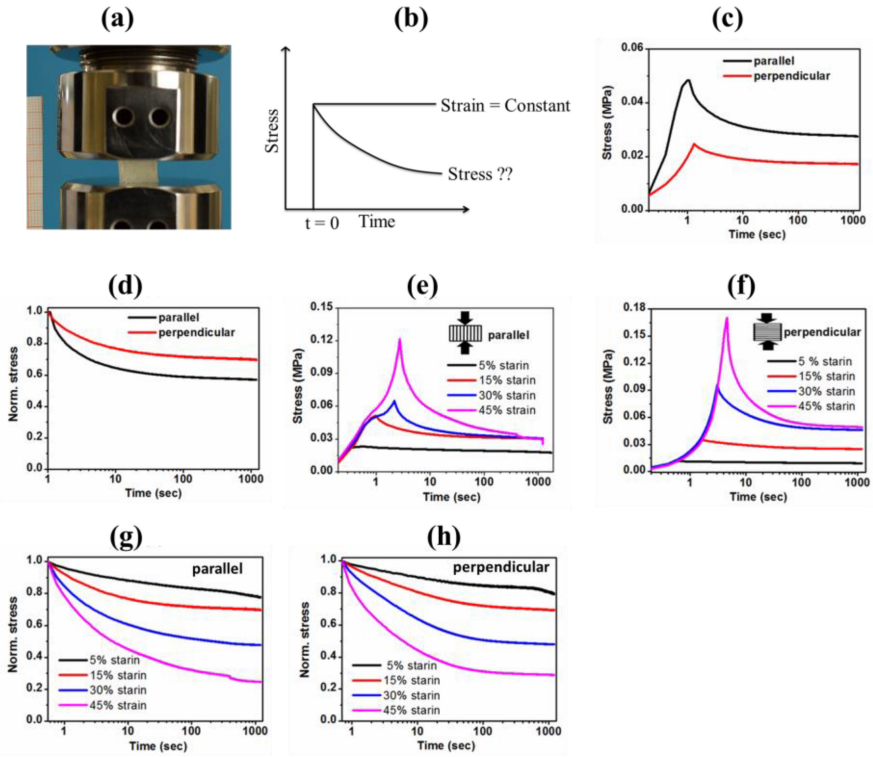

Figure 11. Stress relaxation behaviors of the Gel-PEG hybrid hydrogel: (**a**) representation of stress relaxation test carried out using rectangular-shaped wet samples by being placed between two impermeable metal plates and suddenly subjected to compression up to 15% strain, (**b**) subsequently, the strain is held constant, while the stress is recorded as a function of time, (**c**) stress relaxation behavior of hydrogel is compared compressing in parallel and perpendicular directions, (**d**) corresponding relative rate of relaxation; stress is normalized by the maximum stress, (**e**,**f**) stress relaxation behavior of hydrogel subjected to compression holding at various strain levels (5%, 15%, 30% and 45%) both in parallel and perpendicular directions and (**g**,**h**) corresponding relative rates of relaxation (normalized stress vs. time).

Figure 11c,d represents the comparison of stress relaxation behavior of hydrogel when compressed in parallel and perpendicular directions holding 15% strain and a corresponding relative rate of relaxation, respectively. Clearly, Gel-PEG hydrogel relaxed stress over time. As expected, hydrogel compressed in a parallel direction (relaxation 34 $\pm$ 4% and half stress relaxation time 1 $\pm$ 0.15 s), experienced higher and faster stress relaxation compared to that of a perpendicular direction (relaxation 27 $\pm$ 2% and half stress relaxation time 1.9 $\pm$ 0.3 s). Higher stiffness and movement of more pressurized water might contribute to causing higher and faster relaxation when compressed in a parallel direction.

We further evaluated the trend of stress relaxation rate varying strain levels (5%, 15%, 30% and 45%) at a constant strain rate of 60 mm/min both parallel and perpendicular to

the macroporous channels, as presented in Figure 11e,f. For compression in both directions, the larger the strain, the higher the peak stress (Figure 11e,f), and subsequently, the faster the rate of relaxation (Figure 11g,h). With the increase in deformation level, more water is squeezed out of the hydrogel, resulting in greater hydrogel density, consequently showing higher stress. Denser hydrogel density and faster flow of free water might contribute to relatively higher and faster stress relaxation with increasing deformation levels.

3.4.4. Hydrolytic Mass Loss and Associated Mechanical Properties of Gel-PEG Hybrid Hydrogel

The degradation profile of the hydrogel was assessed by measuring mass loss over time due to hydrolysis. Figure 12a presents the profile of a gradually increasing trend of one-month-long mass loss conducted by incubating the samples in distilled water at 37 °C. Initially, hydrogel lost more mass (~10% at 2 days) due to washing out of the unreacted reagents and dissolving the soluble components. However, afterward, the hydrogel experienced slow hydrolytic degradation. Over the degradation time, hydrolysis of hydrogel cleaved the crosslinked networks, lowered the molecular mass, dissolved into water, and subsequently, increased mass loss.

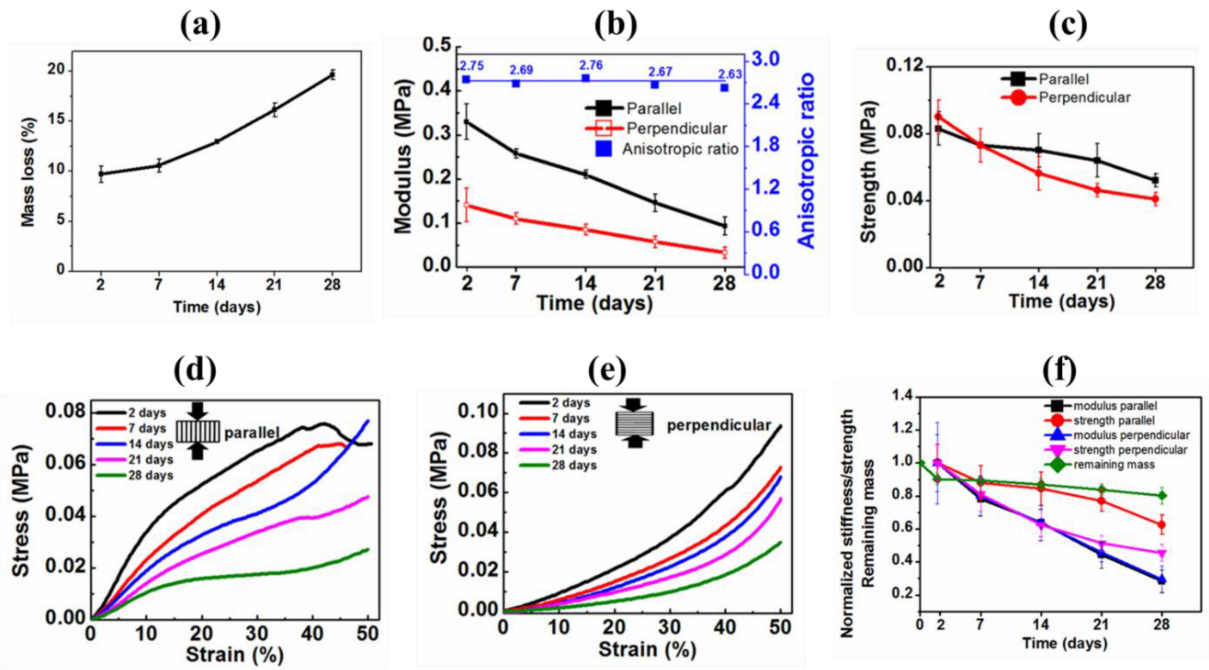

Figure 12. Mass loss (%) and associated mechanical properties of the Gel-PEG hydrogel during hydrolytic degradation in distilled water at 37 °C: (**a**) mass loss (%) of the hydrogel during hydrolytic degradation, (**b**) variation of elastic moduli and anisotropic ratio (blue line) of hydrogel over hydrolysis time, (**c**) variation of strength during hydrolysis time, (**d**,**e**) representative stress-strain curves of hydrogel over hydrolysis time compressed parallel and perpendicular to the macroporous channels, respectively, and finally (**f**) normalized stiffness/strength/remaining mass vs. hydrolysis time.

Again, the hydrolytic degradation of the hydrogel may alter its mechanical property. To assess this hypothesis, the compressive mechanical properties were measured during month-long degradation both in parallel and perpendicular directions, as shown in Table 4 and Figure 12b–f. As expected from the mass loss profile, the stiffness and strength of the hydrogel in both directions gradually decreased over the degradation time due to the polymeric chain scissions of the network reducing the overall crosslinking density. Representative stress-strain curves obtained from various time intervals during degradation also illustrated the gradually decreasing nature of moduli and strengths in both directions, as depicted in Figure 12d,e. We also determined the degradation effect on the anisotropic

ratio of the modulus of the hydrogel. More excitingly, the anisotropic ratio (modulus in parallel direction divided by modulus in perpendicular direction) remained nearly constant during the degradation period, as shown in Table 4 and Figure 12b (blue line). This interesting feature indirectly indicated the uniform and homogeneous degradation of the Gel-PEG hybrid hydrogel, paramount importance for biomedical application, particularly for drug delivery.

Table 4. Trend of mechanical properties variation during degradation period incubated in distilled water at 37 °C.

	Compressed Parallel to the Macroporous Channels		Compressed Perpendicular to the Macroporous Channels		
Time (Days)	**Modulus (MPa)**	**Stress (MPa) at 50% Strain**	**Modulus (MPa)**	**Stress (MPa) at 50% Strain**	**Anisotropic Ratio $E_{\parallel}/E_{\perp}$**
2	0.330 ± 0.04	0.083 ± 0.01	0.120 ± 0.03	0.09 ± 0.01	2.75
7	0.258 ± 0.01	0.073 ± 0.01	0.096 ± 0.01	0.073 ± 0.01	2.69
14	0.211 ± 0.01	0.070 ± 0.01	0.0763 ± 0.01	0.0562 ± 0.01	2.76
21	0.146 ± 0.02	0.064 ± 0.001	0.0548 ± 0.01	0.0462 ± 0.002	2.67
28	0.093 ± 0.02	0.052 ± 0.004	0.0355 ± 0.01	0.0410 ± 0.004	2.63

Stiffness and strength were normalized by the initial stiffness and strength values of 2 days and normalized values were presented as a function of degradation time in Figure 12f. After one month-long hydrolytic degradation, the hydrogel lost ~70% of its initial stiffness in both directions, as observed in Table 4 and Figure 12f. While 45% and 55% initial strength reduction were observed, respectively, in parallel and perpendicular directions. Most importantly, hydrogel maintained good structural stability even after hydrolytic degradation of one month, which is important for long-term in vitro cell behavior or regenerative outcomes. Moreover, the pores generated by degradation will allow more free spaces available for cell growth and proliferation, a most welcome phenomenon for tissue engineering application.

An oversimplified freeze-drying technique was designed to produce highly porous anisotropic 3D Gel-PEG hybrid hydrogel suitable for tissue engineering application. It is known that the higher the cooling rate, the more crystals are formed and the smaller their sizes. Furthermore, the pore sizes of hydrogel are also influenced by the crosslinking density, the type of macromonomers and their hydrophilicity and the molecular weight between crosslinking. We used a freezing temperature of −196 °C to create porous channels along the direction of freezing. The freeze-drying technique produced microporous skin (exterior part of hydrogel), as shown in Figure 3a,d. However, a highly interconnected macroporous structure (distribution of pore sizes within the range of 20–450 μm) was visible beneath the skin, as shown in Figures 3b and 4a–c. Clearly, the freeze-casting strategy used produced two distinct pore morphologies characterized by irregular spherical pore morphology in the cross-section view and channel-like morphology in the side view, resulting in the anisotropic Gel-PEG hydrogel structure. The hydrogel showed a high porosity of 75.12 ± 2.12%. Hydrogel without skin was used for all the characterizations mentioned in this manuscript. The high porosity and a wide range of pore sizes distribution might be used for a wide range of tissue engineering applications. Chengdong ji et al. prepared porous 3D chitosan hydrogel and found that high porosity (porosity 85%) and larger pore volume (pore size > 90 μm) enhanced fibroblast cell viability and proliferation [45]. In another study, Archana Sharma et al. showed that PEG-Gel cryogels with porosity in the range of 75–95% (average pore size in the range of 60–100 μm) provided a suitable microenvironment for the growth and proliferation of different cell types (such as IMR-32 and C2C12) [46].

The tensile stress-strain curve of the Gel-PEG hybrid hydrogel showed a nonlinear stress-strain relationship—a similar response was observed for most of the soft tis-

sues [36,40,41]. The hydrogel showed compressive moduli of 0.33 MPa and 0.12 MPa, respectively, when compressed parallel and perpendicular to the macroporous channels. These moduli are in the same range as native articular cartilage [47–55]. Consecutive cyclic (showed hysteresis loop) and stress relaxation (overall stress relaxed around 30%) tests revealed that the Gel-PEG hydrogel was viscoelastic in nature, which made the hydrogel a potential platform for cartilage tissue engineering [38]. This time-dependent response of the hydrogel is due to the contribution of the viscoelastic behavior of the polymer matrix and water migration through the hydrogel pores [48,56]. The hydrogel showed excellent shape recoverability during the cyclic loading-unloading test. Most importantly, the Gel-PEG hydrogel maintained its mechanical integrity during cyclic compression. Moreover, the maximum stress and dissipation energy of the hydrogel gradually increased with increasing the maximum deformation level; natural cartilage shows the same trend in the cyclic compressive test with increasing strain [49,56–60]. The hydrolytic degradation test exhibited that the hydrogel was degradable. Most interestingly, the Gel-PEG maintained its anisotropic ratio nearly constantly during hydrolytic degradation, indicating a homogeneous degradation profile suitable for many biomedical applications. Thus, all these physical, morphological, and mechanical properties along with the ease of synthesis strategy suggested that the Gel-PEG hybrid hydrogel could be a potential scaffolding material for tissue engineering application.

4. Conclusions

We successfully designed a highly crosslinked hydrolytically degradable Gel-PEG hybrid hydrogel system with anisotropic morphology blessed by highly interconnected porosity and moderate mechanical properties using a benign synthesis approach suitable for a broad range of biomedical applications. We adopted an oversimplified unidirectional freezing technique yet exerted a moderate degree of anisotropy both morphologically and mechanically. The hydrogel system showed outstanding structural stability as well as good mechanical stability and reversibility both in initial and after month-long degradation. We correlated the variation of the anisotropic ratio as a function of degradation time. During the cyclic loading-unloading test, the hydrogel showed a high degree of mechanical stability, which could be beneficial for cartilage tissue engineering. Moreover, the hysteresis loop, percentage dissipation energy and stress-relaxing behavior indicated the viscoelastic nature of the Gel-PEG hybrid hydrogel. Lastly, the impact of anisotropy on the stress relaxation response was established. In one word, this softly-cum-simply-synthesized Gel-PEG hybrid hydrogel possessed promising potential for a wide range of applications including tissue scaffolds and drug delivery devices.

Author Contributions: Conceptualization, K.D. and L.S.; methodology, K.D., S.A. and L.S.; formal analysis, K.D., S.A. and L.S.; investigation, K.D., S.A. and L.S.; data curation, K.D.; writing, K.D.; writing—review and editing, K.D., S.A. and L.S.; visualization, K.D. and L.S.; supervision, S.A. and L.S. All authors have read and agreed to the published version of the manuscript.

Funding: This research received no external funding.

Institutional Review Board Statement: Not applicable.

Informed Consent Statement: Not applicable.

Data Availability Statement: The raw/processed data required to reproduce these findings cannot be shared at this time as the data also form part of an ongoing study.

Acknowledgments: The authors would like to thank Bithi Mojumder at Noakhali Science and Technology University (NSTU), Bangladesh, for the English editing of the manuscript.

Conflicts of Interest: The authors declare no conflict of interest.

References

1. Sadtler, K.; Singh, A.; Wolf, M.T.; Wang, X.; Pardoll, D.M.; Elisseeff, J.H. Design, clinical translation and immunological response of biomaterials in regenerative medicine. *Nat. Rev. Mater.* **2016**, *1*, 16040. [CrossRef]
2. Giwa, S.; Lewis, J.K.; Alvarez, L.; Langer, R.; Roth, A.E.; Church, G.M.; Markmann, J.F.; Sachs, D.H.; Chandraker, A.; Wertheim, J.A.; et al. The promise of organ and tissue preservation to transform medicine. *Nat. Biotechnol.* **2017**, *35*, 530–542. [CrossRef] [PubMed]
3. World Health Organization (WHO). Transplantation. Available online: https://www.who.int/health-topics/transplantation#tab=tab_2 (accessed on 15 January 2023).
4. Dey, K.; Agnelli, S.; Re, F.; Russo, D.; Lisignoli, G.; Manferdini, C.; Bernardi, S.; Gabusi, E.; Sartore, L. Rational Design and Development of Anisotropic and Mechanically Strong Gelatin—Based Stress Relaxing Hydrogels for Osteogenic/Chondrogenic Differentiation. *Macromol. Biosci.* **2019**, *19*, 1900099. [CrossRef]
5. Dey, K.; Roca, E.; Ramorino, G.; Sartore, L. Progress in the mechanical modulation of cell functions in tissue engineering. *Biomater. Sci.* **2020**, *8*, 7033–7081. [CrossRef]
6. Slaughter, B.V.; Khurshid, S.S.; Fisher, O.Z.; Khademhosseini, A.; Peppas, N.A. Hydrogels in regenerative medicine. *Adv. Mater.* **2009**, *21*, 3307–3329. [CrossRef]
7. Khademhosseini, A.; Langer, R.; Borenstein, J.; Vacanti, J.P. Microscale technologies for tissue engineering and biology. *Proc. Natl. Acad. Sci. USA* **2006**, *103*, 2480–2487. [CrossRef]
8. Dey, K.; Agnelli, S.; Serzanti, M.; Ginestra, P.; Scarì, G.; Dell'Era, P.; Sartore, L. Preparation and properties of high performance gelatin-based hydrogels with chitosan or hydroxyethyl cellulose for tissue engineering applications. *Int. J. Polym. Mater. Polym. Biomater.* **2018**, *68*, 183–192. [CrossRef]
9. Elkhoury, K.; Russell, C.S.; Sanchez-Gonzalez, L.; Mostafavi, A.; Williams, T.J.; Kahn, C.; Peppas, N.A.; Arab-Tehrany, E.; Tamayol, A. Soft-Nanoparticle functionalization of natural hydrogels for tissue engineering applications. *Adv. Healthc. Mater.* **2019**, *8*, 1900506. [CrossRef]
10. Joyce, K.; Fabra, G.T.; Bozkurt, Y.; Pandit, A. Bioactive potential of natural biomaterials: Identification, retention and assessment of biological properties. *Signal Transduct. Target. Ther.* **2021**, *6*, 122. [CrossRef]
11. Jia, X.; Kiick, K.L. Hybrid multicomponent hydrogels for tissue engineering. *Macromol. Biosci.* **2009**, *9*, 140–156. [CrossRef]
12. Cai, M.H.; Chen, X.Y.; Fu, L.Q.; Du, W.L.; Yang, X.; Mou, X.Z.; Hu, P.Y. Design and development of hybrid hydrogels for biomedical applications: Recent trends in anticancer drug delivery and tissue engineering. *Front. Bioeng. Biotechnol.* **2021**, *9*, 630943. [CrossRef] [PubMed]
13. Lin, X.; Xing, X.; Li, S.; Wu, X.; Jia, Q.; Tu, H.; Bian, H.; Lu, A.; Zhang, L.; Yang, H.; et al. Anisotropic Hybrid Hydrogels Constructed via the Noncovalent Assembly for Biomimetic Tissue Scaffold. *Adv. Funct. Mater.* **2022**, *32*, 2112685. [CrossRef]
14. Sun, L.; Chen, Z.; Xu, D.; Zhao, Y. Electroconductive and Anisotropic Structural Color Hydrogels for Visual Heart-on-a-Chip Construction. *Adv. Sci.* **2022**, *9*, 2105777. [CrossRef] [PubMed]
15. Chau, M.; De France, K.J.; Kopera, B.; Machado, V.R.; Rosenfeldt, S.; Reyes, L.; Chan, K.J.; Forster, S.; Cranston, E.D.; Hoare, T.; et al. Composite hydrogels with tunable anisotropic morphologies and mechanical properties. *Chem. Mater.* **2016**, *28*, 3406–3415. [CrossRef]
16. Choi, S.; Choi, Y.; Kim, J. Anisotropic hybrid hydrogels with superior mechanical properties reminiscent of tendons or ligaments. *Adv. Funct. Mater.* **2019**, *29*, 1904342. [CrossRef]
17. Proksch, E.; Brandner, J.M.; Jensen, J.M. The skin: An indispensable barrier. *Exp. Dermatol.* **2008**, *17*, 1063–1072. [CrossRef]
18. Engelmayr, G.C.; Cheng, M.; Bettinger, C.J.; Borenstein, J.T.; Langer, R.; Freed, L.E. Accordion-like honeycombs for tissue engineering of cardiac anisotropy. *Nat. Mater.* **2008**, *7*, 1003–1010. [CrossRef]
19. Sano, K.; Ishida, Y.; Aida, T. Synthesis of anisotropic hydrogels and their applications. *Angew. Chem. Int. Ed.* **2018**, *57*, 2532–2543. [CrossRef]
20. Sophia Fox, A.J.; Bedi, A.; Rodeo, S.A. The basic science of articular cartilage: Structure, composition, and function. *Sport. Health* **2009**, *1*, 461–468. [CrossRef]
21. Marelli, B.; Ghezzi, C.E.; James-Bhasin, M.; Nazhat, S.N. Fabrication of injectable, cellular, anisotropic collagen tissue equivalents with modular fibrillar densities. *Biomaterials* **2015**, *37*, 183–193. [CrossRef]
22. Chen, M.; Zhu, J.; Qi, G.; He, C.; Wang, H. Anisotropic hydrogels fabricated with directional freezing and radiation-induced polymerization and crosslinking method. *Mater. Lett.* **2012**, *89*, 104–107. [CrossRef]
23. Li, T.; Hou, J.; Wang, L.; Zeng, G.; Wang, Z.; Yu, L.; Yang, Q.; Yin, J.; Long, M.; Chen, L.; et al. Bioprinted anisotropic scaffolds with fast stress relaxation bioink for engineering 3D skeletal muscle and repairing volumetric muscle loss. *Acta Biomater.* **2023**, *156*, 21. [CrossRef]
24. Zhu, J. Bioactive modification of poly (ethylene glycol) hydrogels for tissue engineering. *Biomaterials* **2010**, *31*, 4639–4656. [CrossRef]
25. Khuu, N.; Kheiri, S.; Kumacheva, E. Structurally anisotropic hydrogels for tissue engineering. *Trends Chem.* **2021**, *3*, 1002. [CrossRef]
26. Chen, Z.; Khuu, N.; Xu, F.; Kheiri, S.; Yakavets, I.; Rakhshani, F.; Morozova, S.; Kumacheva, E. Printing Structurally Anisotropic Biocompatible Fibrillar Hydrogel for Guided Cell Alignment. *Gels* **2022**, *8*, 685. [CrossRef]

27. Wang, M.; Yang, C.; Deng, H.; Du, Y.; Xiao, L.; Shi, X. Electrically induced anisotropic assembly of chitosan with different molecular weights. *Carbohydr. Polym.* **2023**, *304*, 120494. [CrossRef]
28. Wang, C.; Pan, Z.Z.; Lv, W.; Liu, B.; Wei, J.; Lv, X.; Luo, Y.; Nishihara, H.; Yang, Q.H. A directional strain sensor based on anisotropic microhoneycomb cellulose nanofiber-carbon nanotube hybrid aerogels prepared by unidirectional freeze drying. *Small* **2019**, *15*, 1805363. [CrossRef]
29. Mredha, M.T.I.; Jeon, I. Biomimetic anisotropic hydrogels: Advanced fabrication strategies, extraordinary functionalities, and broad applications. *Prog. Mater. Sci.* **2022**, *124*, 100870. [CrossRef]
30. Chen, Q.; Zhang, X.; Chen, K.; Wu, X.; Zong, T.; Feng, C.; Zhang, D. Anisotropic hydrogels with enhanced mechanical and tribological performance by magnetically oriented nanohybrids. *Chem. Eng. J.* **2022**, *430*, 133036. [CrossRef]
31. Xing, J.; Liu, N.; Xu, N.; Chen, W.; Xing, D. Engineering complex anisotropic scaffolds beyond simply uniaxial alignment for tissue engineering. *Adv. Funct. Mater.* **2022**, *32*, 2110676. [CrossRef]
32. Wang, W.; Deng, X.; Luo, C. Anisotropic hydrogels with high-sensitivity and self-adhesion for wearable sensors. *J. Mater. Chem. C* **2023**, *11*, 196–203. [CrossRef]
33. Huang, J.; Wu, D.; Xiong, X. Preparation of a composite hydrogel of polyvinyl alcohol/chitosan fiber with anisotropic properties for sustained drug release. *J. Appl. Polym. Sci.* **2022**, *139*, e53199. [CrossRef]
34. Wang, L.; Li, T.; Wang, Z.; Hou, J.; Liu, S.; Yang, Q.; Yu, L.; Guo, W.; Wang, Y.; Guo, B.; et al. Injectable remote magnetic nanofiber/hydrogel multiscale scaffold for functional anisotropic skeletal muscle regeneration. *Biomaterials* **2022**, *285*, 121537. [CrossRef] [PubMed]
35. Tognato, R.; Bonfrate, V.; Giancane, G.; Serra, T. Fabrication of anisotropic collagen-based substrates for potential use in tissue engineering. *Smart Mater. Struct.* **2022**, *31*, 074001. [CrossRef]
36. Dey, K.; Agnelli, S.; Borsani, E.; Sartore, L. Degradation-Dependent Stress Relaxing Semi-Interpenetrating Networks of Hydroxyethyl Cellulose in Gelatin-PEG Hydrogel with Good Mechanical Stability and Reversibility. *Gels* **2021**, *7*, 277. [CrossRef]
37. Dey, K.; Agnelli, S.; Sartore, L. Effects of gamma sterilization on the physicomechanical and thermal properties of gelatin-based novel hydrogels. *Polym. Eng. Sci.* **2019**, *59*, 2533–2540. [CrossRef]
38. Dey, K.; Agnelli, S.; Sartore, L. Dynamic freedom: Substrate stress relaxation stimulates cell responses. *Biomater. Sci.* **2019**, *7*, 836–842. [CrossRef]
39. Yu, S.; Liu, J.; Wei, M.; Luo, Y.; Zhu, X.; Liu, Y. Compressive property and energy absorption characteristic of open-cell ZA22 foams. *Mater. Des.* **2009**, *30*, 87–90. [CrossRef]
40. Suhr, J.; Victor, P.; Ci, L.; Sreekala, S.; Zhang, X.; Nalamasu, O.; Ajayan, P.M. Fatigue resistance of aligned carbon nanotube arrays under cyclic compression. *Nat. Nanotechnol.* **2007**, *2*, 417–421. [CrossRef]
41. Chaudhuri, O.; Gu, L.; Klumpers, D.; Darnell, M.; Bencherif, S.A.; Weaver, J.C.; Huebsch, N.; Lee, H.P.; Lippens, E.; Duda, G.N.; et al. Hydrogels with tunable stress relaxation regulate stem cell fate and activity. *Nat. Mater.* **2016**, *15*, 326–334. [CrossRef]
42. Bernardi, S.; Re, F.; Bosio, K.; Dey, K.; Almici, C.; Malagola, M.; Guizzi, P.; Sartore, L.; Russo, D. Chitosan-Hydrogel polymeric scaffold acts as an independent primary inducer of osteogenic differentiation in human mesenchymal stromal cells. *Materials* **2020**, *13*, 3546. [CrossRef]
43. Re, F.; Sartore, L.; Moulisova, V.; Cantini, M.; Almici, C.; Bianchetti, A.; Chinello, C.; Dey, K.; Agnelli, S.; Manferdini, C.; et al. 3D gelatin-chitosan hybrid hydrogels combined with human platelet lysate highly support human mesenchymal stem cell proliferation and osteogenic differentiation. *J. Tissue Eng.* **2019**, *10*, 2041731419845852. [CrossRef]
44. Manferdini, C.; Gabusi, E.; Sartore, L.; Dey, K.; Agnelli, S.; Almici, C.; Bianchetti, A.; Zini, N.; Russo, D.; Re, F.; et al. Chitosan-based scaffold counteracts hypertrophic and fibrotic markers in chondrogenic differentiated mesenchymal stromal cells. *J. Tissue Eng. Regen. Med.* **2019**, *13*, 1896–1911. [CrossRef]
45. Ji, C.; Khademhosseini, A.; Dehghani, F. Enhancing cell penetration and proliferation in chitosan hydrogels for tissue engineering applications. *Biomaterials* **2011**, *32*, 9719. [CrossRef]
46. Sharma, A.; Bhat, S.; Nayak, V.; Kumar, A. Efficacy of supermacroporous poly (ethylene glycol)–gelatin cryogel matrix for soft tissue engineering applications. *Mater. Sci. Eng. C* **2015**, *47*, 298. [CrossRef]
47. Gu, L.; Li, T.; Song, X.; Yang, X.; Li, S.; Chen, L.; Liu, P.; Gong, X.; Chen, C.; Sun, L. Preparation and characterization of methacrylated gelatin/bacterial cellulose composite hydrogels for cartilage tissue engineering. *Regen. Biomater.* **2020**, *7*, 195. [CrossRef]
48. Todros, S.; Spadoni, S.; Barbon, S.; Stocco, E.; Confalonieri, M.; Porzionato, A.; Pavan, P.G. Compressive Mechanical Behavior of Partially Oxidized Polyvinyl Alcohol Hydrogels for Cartilage Tissue Repair. *Bioengineering* **2022**, *9*, 789. [CrossRef]
49. Li, W.; Wang, D.; Yang, W.; Song, Y. Compressive mechanical properties and microstructure of PVA–HA hydrogels for cartilage repair. *RSC Adv.* **2016**, *6*, 20166. [CrossRef]
50. Wang, W.; Shi, Y.; Lin, G.; Tang, B.; Li, X.; Zhang, J.; Ding, X.; Zhou, G. Advances in mechanical properties of hydrogels for cartilage tissue defect repair. *Macromol. Biosci.* **2023**, 2200539. [CrossRef]
51. Taheri, S.; Ghazali, H.S.; Ghazali, Z.S.; Bhattacharyya, A.; Noh, I. Progress in biomechanical stimuli on the cell-encapsulated hydrogels for cartilage tissue regeneration. *Biomater. Res.* **2023**, *27*, 22. [CrossRef]
52. Zhu, C.; Zhang, W.; Shao, Z.; Wang, Z.; Chang, B.; Ding, X.; Yang, Y. Biodegradable glass fiber reinforced PVA hydrogel for cartilage repair: Mechanical properties, ions release behavior and cell recruitment. *J. Mat. Res. Technol.* **2023**, *23*, 154. [CrossRef]

53. Demott, C.J.; Jones, M.R.; Chesney, C.D.; Yeisley, D.J.; Culibrk, R.A.; Hahn, M.S.; Grunlan, M.A. Ultra-High modulus hydrogels mimicking cartilage of the human body. *Macromol. Biosci.* **2022**, *22*, 2200283. [CrossRef] [PubMed]
54. Wu, Y.; Li, X.; Wang, Y.; Shi, Y.; Wang, F.; Lin, G. Research progress on mechanical properties and wear resistance of cartilage repair hydrogel. *Mater. Des.* **2022**, *216*, 110575. [CrossRef]
55. Benitez-Duif, P.A.; Breisch, M.; Kurka, D.; Edel, K.; Gökcay, S.; Stangier, D.; Tillmann, W.; Hijazi, M.; Tiller, J.C. Ultrastrong poly (2-oxazoline)/poly (acrylic acid) double-network hydrogels with cartilage-like mechanical properties. *Adv. Funct. Mater.* **2022**, *32*, 2204837. [CrossRef]
56. Romischke, J.; Scherkus, A.; Saemann, M.; Krueger, S.; Bader, R.; Kragl, U.; Meyer, J. Swelling and mechanical characterization of polyelectrolyte hydrogels as potential synthetic cartilage substitute materials. *Gels* **2022**, *8*, 296. [CrossRef]
57. Hao, M.; Wang, Y.; Li, L.; Liu, Y.; Bai, Y.; Zhou, W.; Lu, Q.; Sun, F.; Li, L.; Feng, S.; et al. Tough engineering hydrogels based on swelling–freeze–thaw method for artificial cartilage. *ACS Appl. Mater. Interfaces* **2022**, *14*, 25093. [CrossRef]
58. Choi, J.H.; Kim, J.S.; Kim, W.K.; Lee, W.; Kim, N.; Song, C.U.; Jung, J.J.; Song, J.E.; Khang, G. Evaluation of hyaluronic acid/agarose hydrogel for cartilage tissue engineering biomaterial. *Macromol. Res.* **2020**, *28*, 979. [CrossRef]
59. Lee, S.; Choi, J.; Youn, J.; Lee, Y.; Kim, W.; Choe, S.; Song, J.; Reis, R.L.; Khang, G. Development and evaluation of gellan gum/silk fibroin/chondroitin sulfate ternary injectable hydrogel for cartilage tissue engineering. *Biomolecules* **2021**, *11*, 1184. [CrossRef]
60. Phatchayawat, P.P.; Khamkeaw, A.; Yodmuang, S.; Phisalaphong, M. 3D bacterial cellulose-chitosan-alginate-gelatin hydrogel scaffold for cartilage tissue engineering. *Biochem. Eng. J.* **2022**, *184*, 108476. [CrossRef]

Disclaimer/Publisher's Note: The statements, opinions and data contained in all publications are solely those of the individual author(s) and contributor(s) and not of MDPI and/or the editor(s). MDPI and/or the editor(s) disclaim responsibility for any injury to people or property resulting from any ideas, methods, instructions or products referred to in the content.